

# Design and Performance Test of an Indigenously Fabricated Sub-sonic Wind Tunnel

Muhammad Adeel<sup>a</sup>, Abdul Hameed Memon<sup>b</sup>, Syed Raheel Zafar<sup>c</sup>, Saad Bin Ishtiaq<sup>c</sup>,  
Muhammad Hassaan Ali<sup>c</sup> and Ahmed Hussain<sup>d\*</sup>

<sup>a</sup>Department of Mechatronics Engineering, SABIST, Karachi, Pakistan

<sup>b</sup>Department of Mechanical Engineering, Faculty of Engineering Sciences and Technology (FEST),  
Hamdard University, Karachi, Pakistan

<sup>c</sup>Department of Mechanical Engineering, DHA Suffa University, Karachi, Pakistan

<sup>d</sup>Department of Nuclear Engineering, Kind Abdulaziz University, Jeddah, Saudi Arabia

(received February 24, 2019; revised March 26, 2021; accepted April 2, 2021)

---

**Abstract.** The study of the interaction between wind flow and the surface is crucial to many applications including industry, automotive and most importantly aerospace. Computational Fluid Dynamics (CFD) has come a long way in the last couple of decades but still experimental validations of its results are required. Therefore, development of a small-scale low-cost subsonic wind tunnel is proposed in this project, with the aim that the final product can be used as a laboratory equipment and for further research and design projects. In the proposed project, a low-cost easy to manufacture subsonic wind tunnel is designed and fabricated. A study of various designs of wind tunnels including both open loop and closed loop wind tunnels is performed. The size of the proposed wind tunnel would be determined such that it can be easily accommodated in our laboratory. The calculations based on these constraints is carried out using the requirement of flow match number and the governing equations such as the continuity equation and Bernoulli's equation. An additional component can be added using CFD to analyze and validate the flow regime in the test section based on the design.

**Keywords:** computational fluid dynamics, subsonic wind tunnel, flow regime, design, match number

---

## Introduction

The fields of aerodynamics and fluid mechanics have received an immense amount of attention both with respect to research and development within the last few decades, the change in the behaviour of flow towards a different type of shapes and structures are studied under these domains (Maurya *et al.*, 2018). However, theoretical techniques are not sufficient to provide accurate results, this can be due to the complex problems or complex flow of the fluid and hence the results are sometimes impossible to obtain without proper experimentation (Almeida *et al.*, 2018). In such cases, wind tunnels are used to study the behavior of fluids. Many types of wind tunnels are created depending upon the task to be tackled, among many wind tunnels the sub-sonic wind tunnel equipment deals with the fluid being operated at a velocity below the speed of sound (Abdelhamed *et al.*, 2015). The wind tunnel can provide the researchers a wide range of possibilities to test different types of airfoils, to check their aerodynamics performance for *e.g.* lift drag and flow behavior etc (Parpanchi *et al.*, 2021). Furthermore, the research has

\*Author for correspondence; E-mail: ahassain@kau.edu.sa

expanded to almost all fields of science including architecture, automotive industry, education, environment etc. (Hernandez *et al.*, 2013; Lerner and Boldes *et al.*, 2011). Wind tunnels because of the circuit design can be classified as 'open loop' and 'closed loop' wind tunnel (Verma and Baloni, 2018). Each wind tunnel is designed with a specific range of flow speed in mind and therefore wind tunnels can be classified based on the flow speed of working fluid, it can be 'sub-sonic', 'super-sonic', 'trans-sonic', or 'hypersonic'. The fluid flow can be turbulent or laminar in nature and based on requirement the wind tunnels can be designed to cater either type. The nature of flow can be obtained by Reynolds number (Eugeni *et al.*, 2020). Wind tunnel provides a variety of options to experiment with fluid flow and its effects on test specimens, the classification of wind tunnel is done on the basis of purpose of aerodynamic flow, wind resistance and improving energy consumptions, study of flow patterns, and proof of basic concepts related to torque, pressure, velocity, etc. (Madara *et al.*, 2017). Wind tunnels have been in use for a long time. The Wright brothers used a small scale open-loop wind tunnel, with a 16-inch test section

for their experiments; this was back in 1871 (Joglekar and Mourya, 2014; Singh *et al.*, 2013). Gradually, their size increased and so did their complexity, by 1909 different wind tunnels were being made for different purposes, for example, the altitude wind tunnel, which tried to replicate the altitude conditions to study engine performance in altitude conditions (Leifsson and Koziel, 2015; Riazi and Ahmed, 2011). The design is shown in Fig. 1.

Subsonic wind tunnels are usually dedicated for experimentation at low subsonic regimes ( $M < 0.4$  or  $134\text{m/s}$ ). Here compressibility effects are generally negligible. They may be open return type (Eiffel type) or closed return type (Prandtl type). Open and close types have their own requirements and configurations. Since Open types are generally used for educational purpose, where cost matters although closed types are generally preferred by researchers, where quality matters. High speed tunnels ( $0.4 < M < 0.8$ ) and transonic tunnels ( $0.8 < M < 1.2$ ) are both designed on the same principles as subsonic tunnels. Here compressibility factors matter a lot and in transonic tunnels, there have been shocks inside a test section so perforated walls are being used to reduce shock reflections (Abdelhamed *et al.*, 2015).

The effects of the fluctuations in velocities are being modeled by solving the momentum equations and also the modeling of turbulence equations. The Mixture Turbulence Model (MTM) turbulence model is being used for our simulations. The k-turbulence model turbulence is used for the air flow in the test section. The turbulent kinetic energy and its dissipation rate are



**Fig. 1.** Wright brothers wind tunnel.

solved by k-model. The governing equations were discretized using the finite volume technique and were solved to obtain a numerical solution.

**Materials and Methods**

The design procedure mainly depends on the specification, requirements, and cost of the overall wind tunnel. For educational purposes, the flow quality can be compromised thus reducing the overall cost of the wind tunnel whereas the opposite is true for research and aeronautical application. The main design specifications of the wind tunnel which has to be defined before starting the design are flow velocity inside the test section, the quality of the flow required in the test section and the overall size of the wind tunnel. In order to start the design procedure, the following procedure has been recommended (Nguyen, 2014). By far the most important design criterion for a wind tunnel is its test section. A bigger test section would mean the wind tunnel is going to be big as well. Riazi and Ahmed (2011) have discussed the design of low-speed wind tunnels as well as their common usage and their classifications including the wind tunnels with maximum speed capability up to about 300 mph,  $Mach = 0.4$  (Mashud, 2012). Primary dimension criteria of the test section is its hydraulic diameter, which leads to its cross-sectional area ( $A_{ts}$ ), and hydraulic diameter,  $D_{h(ts)}$  relation given in equation:

$$A_{ts} = \frac{\pi D_{h(ts)}^2}{4} \dots\dots\dots (1)$$

$$D_{h(ts)} = 2 \sqrt{\frac{\pi}{4}} \dots\dots\dots (2)$$

The shape of the test section should be based on the utility and considerations of the aerodynamic model to be tested. If the edges are not chamfered an eddy will be generated due to flow separation.

$$L_{ts} = \left(\frac{0.5}{3}\right) \times D_{h(ts)} \dots\dots\dots (3)$$

where:

$L_{ts}$  = Length of the test section.

A test chamber of length 2 times its hydraulic diameter is the optimum value in the wind tunnel design.

**Table 1.** Test section characteristics

$D_{h(ts)}$	0.2 m
$A_{ts}$	0.04 m
$L_{ts}$	0.4 m

In the context of wind tunnels, measurements of model drag can be used to predict the corresponding drag, on the prototype. If the same fluid is used for model and prototype ( $v_m = v$ ) so that and, therefore, the required model velocity will be higher than the prototype velocity for  $(\frac{1}{l_m})$  greater than 1. Since this ratio is often relatively large, the required value of  $v_m$  may be large. Comparing Reynolds number (Rem) equation of model (m) and prototype:

$$Re_m = Re$$

$$\frac{\rho_m V_m l_m}{\mu_m} = \frac{\rho v l}{\mu}$$

$$V_m = \frac{\mu_m}{\mu} \frac{\rho}{\rho_m} \frac{1}{l_m} V$$

$$V_m = \frac{v_m}{v} \frac{1}{l_m} V$$

where:

$\frac{v}{v_m}$  ratio of kinematic viscosity

The ratio of kinematic viscosity may be taken as one as there is no compressibility effect expected in a low-speed wind tunnel as it is not pressurised.

$$V_m = \frac{1}{l_m} V \dots\dots\dots (4)$$

For a typical large scale subsonic wind tunnel, the length of the test section is 1.25 m and the velocity ranges from 12-24 m/s (Kumar *et al.*, 2012). For our model, the length of the test section is 0.3 m. Therefore,

$$V_m = \frac{1.25}{0.3} \times 12$$

$$V_m - 50 \text{ m/s}$$

The required model velocity can also be reduced if the length scale is modest; that is, the model is relatively large. Design of the contraction cone plays a vital role to maintain the uniform flow in the chamber. The tail end of the contraction cone has a similar cross-section as the test section. The nozzle exit section along with the sharp edges of the contraction cone has 45° chamfer.

Using the fifth order Bell and Mehta polynomial (Hernandez *et al.*, 2011).

$$y = a_1 \epsilon^5 + a_2 \epsilon^4 + a_3 \epsilon^3 + a_4 \epsilon^2 + a_5 \epsilon + C \dots\dots (5)$$

$$\epsilon = \frac{x}{L} \dots\dots\dots (6)$$

where:

$\epsilon$  is the ratio between x coordinate and the total nozzle length and  $a_i$  are the polynomial coefficients.

Null values of the second derivative of the BELL-MEHTA polynomial). These conditions are shown in from equation 7 to 11 for the inlet section and equation 12 for the outlet.

$$\epsilon = 0 \rightarrow y = y_0 \dots\dots\dots (7)$$

$$\epsilon = 1 \rightarrow y = y_1 \dots\dots\dots (8)$$

$$\epsilon = 0 \rightarrow \frac{dy}{d\zeta} = 0 \dots\dots\dots (9)$$

$$\epsilon = 1 \rightarrow \frac{dy}{d\zeta} = 0 \dots\dots\dots (10)$$

$$\epsilon = 0 \rightarrow \frac{d^2y}{d\zeta^2} = 0 \dots\dots\dots (11)$$

$$\epsilon = 1 \rightarrow \frac{d^2y}{d\zeta^2} = 0 \dots\dots\dots (12)$$

As far as the longitudinal-section nozzle profile is concerned, by using the Bell-Mehta fifth order polynomial (Paper *et al.*, 2012) we have:

$$\frac{L}{2y_0} = 1 \dots\dots\dots (13)$$

After solving the equation 13 and by applying all the conditions we get the following coefficients.

The points for the curve are obtained by incorporating equation 4 into a MATLAB program. The curve obtained from that MATLAB function is given in Fig. 2.

The results obtained are shown in Table 3.

The function of a diffuser is to slow down the flow speed so that pressure losses are minimized. Diffuser provides a guide for the air from the test section to the fan. During the procurement of a fan, one should get

**Table 2.** Coefficients of fifth order polynomial equation

Coefficient	Value
$\alpha_1$	$6(y_1-y_0)$
$\alpha_2$	$-15(y_1-y_0)$
$\alpha_3$	$10(y_1-y_0)$
$\alpha_4$	0
$\alpha_5$	0
C	$y_0$

one with as much airflow as possible (and which is affordable) with a large diameter. The transition between the test section and fan should be gentle, so we get the long gradual slope. If the slope and transition are dramatic, the airflow will separate from the walls and turbulence is created which according to (Blevins, 1986) this ratio should be between 2 and 3. Following is the equation:

$$2 \leq AR = \frac{A_{fan}}{A_{TS}} \leq 3 \dots\dots\dots (14)$$

where:

AR = Area ratio of the diffuser.

The fan diameter can be found by knowing the area ratio and the outlet diffuser cross-section area ( $A_{TS}$ ).

$$D_{fan} = 2 \sqrt{\frac{AR A_{TS}}{\pi}} \dots\dots\dots (15)$$

where:

$D_{fan}$  = diameter of the fan at the outlet.

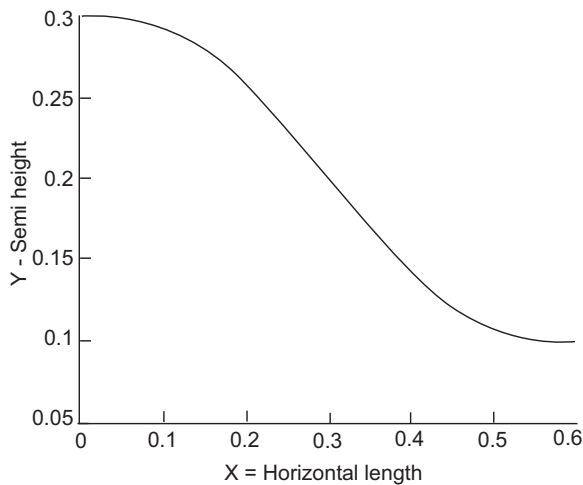


**Fig. 2.** Fifth-order polynomial curve representing the contraction Silhouette generated using MATLAB to describe the wall profile of the Nozzle.

**Table 3.** Nozzle characteristics

Contraction ratio	CR	9
Hydraulic diameter at the inlet of nozzle	$D_h$	0.6
Length of the nozzle	L	0.6

$$a = \tan^{-1} \frac{1}{2} \frac{\sqrt{AR-1}}{\frac{L_{Diff}}{D_h}} \dots\dots\dots (16)$$

If we use 8° Cone expansion angle there will be flow detachment and immense turbulence. The model of the said diffuser is shown Fig. 3. If we use 4° angle the flow detachment will be less, which is desirable for us (Findanis *et al.*, 2011). The diffuser characteristics are given in Table 4.

Before fluid entering the nozzle, there is a settling chamber with the constant cross-sectional area (Ahmed, 2010).

$$\beta_h = \frac{\Omega_{flow}}{\Omega_{tot}} \dots\dots\dots (17)$$

where:

$\beta_h$  = honeycomb porosity

$\Omega_{flow}$  = honeycomb actual flow cross sectional area

$\Omega_{tot}$  = total cross sectional area of the honeycomb.

The honeycomb structure is shown in Fig. 4. (Lien and Ahmed, 2011).

$$6 \leq \frac{L_{honey}}{D_{h \text{ honey}}} \leq 8$$

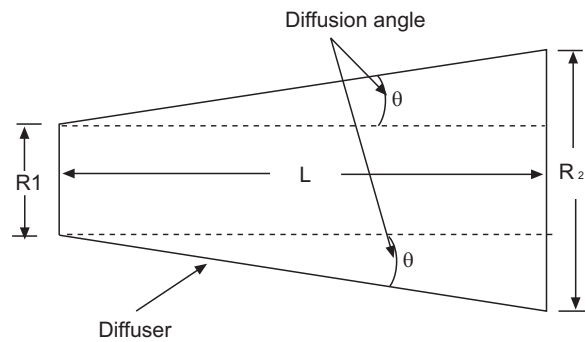


**Fig. 3.** Diffusion angle shown in a model diffuser.

**Table 4.** Diffuser characteristics

Area inlet for diffuser	$A_i$	0.03142 (m <sup>2</sup> )
Inlet hydraulic diameter	$D_{h i}$	0.2 (m)
Area ratio	AR	3
Area exit of the diffuser	$A_e$	0.096 (m <sup>2</sup> )
Diffuser expansion angle	$\alpha/2$	3°
Length of the diffuser	L	1.4 (m)
Exit diameter of diffuser	$D_{h e}$	0.35 (m)

$$\beta_h \geq 0.8$$

$$l_{\text{honey}} = \frac{d_{\text{honey}}}{2 \sin 60} \dots\dots\dots (18)$$

$$l_{g \text{ honey}} = l_{\text{honey}} + 2 \frac{S_{\text{honey}}}{\tan 60} \dots\dots\dots (19)$$

Using the same method the solid sheet division can be easily evaluated in equation 20.

$$z l_{\text{honey}} = 2l_{\text{honey}} + 2l_{g \text{ honey}} \dots\dots\dots (20)$$

$$S_{\text{rectangle}} = l_{\text{honey}} S_{\text{honey}} \dots\dots\dots (21)$$

$$S_{\text{trapeze}} = \frac{(l_{\text{honey}} + l_{g \text{ honey}}) S_{\text{honey}}}{2} \dots\dots\dots (22)$$

$$n_z = \frac{h_{sc}}{z_{\text{honey}}} \dots\dots\dots (23)$$

where:

$n_z$  = no. of divisions height wise

$h_{sc}$  = settling chamber cross section height

$z_{\text{honey}}$  = honey comb divisions.

$$n_{\text{sheet}} = \frac{L_{sc}}{S_{\text{honey}} + \frac{d_{\text{honey}}}{2}} \dots\dots\dots (24)$$

It is evident that for square cross-section equation 25.

$$h_{sc} = L_{sc} \dots\dots\dots (25)$$

Therefore, the cross-section area of the honeycomb solid sheet is calculated using in equation 26 comes out.

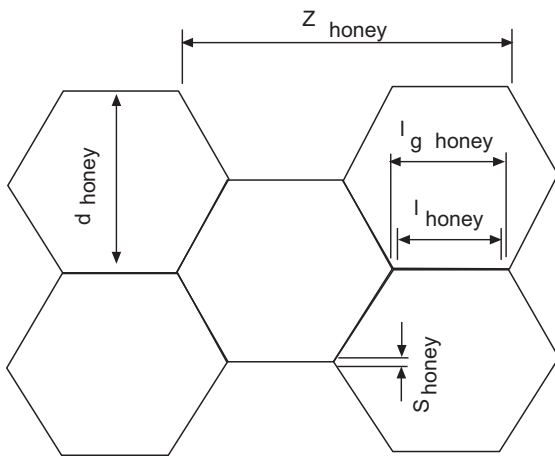


Fig. 4. Honeycomb structure.

$$A_{\text{sheet}} = 2 (S_{\text{rectangle}} + S_{\text{trapeze}}) n_z n_{\text{sheet}} \dots\dots (26)$$

According to the solidity definition equation 27 comes out.

$$\sigma_h = \frac{A_{\text{sheet}}}{A_{\text{total}}} \dots\dots\dots (27)$$

It is easy to achieve the conclusion that the honeycomb solidity  $\sigma_h$  are complementary factors  $\beta_h$ . Thus equation 28 comes out.

$$\sigma_h + \beta_h = 1 \dots\dots\dots (28)$$

Firstly, the cell area is calculated using equation 29.

$$A_{\text{cell}} = \frac{3}{2} \frac{d_{\text{honey}}^2}{\sqrt{3}} \dots\dots\dots (29)$$

Areas equality is used to determine the cell hydraulic diameter in equation 30.

$$\pi \frac{D_{h \text{ honey}}^2}{4} = \Omega_{\text{cell}} = \frac{3}{2} \frac{d_{\text{honey}}^2}{\sqrt{3}} \dots\dots\dots (30)$$

Thus equation 31 comes out and the hydraulic diameter can be calculated.

$$D_{h \text{ honey}} = D_{h \text{ honey}} \sqrt{\frac{6}{\pi \sqrt{3}}} \dots\dots\dots (31)$$

Both the criteria expressed at the start of honeycomb must be verified at the end of the honeycomb design procedure. The honey characteristics are tabulated in Table 5.

The screen porosity,  $\beta_s$ , is usually defined as the actual flow area and total area ratio equation 33 (Ahmed, 2012).

$$\beta_s = \frac{A_{\text{flow}}}{A_{\text{tot}}} \dots\dots\dots (32)$$

Therefore, the screening effectiveness is as shown in equation 33.

Table 5. Honeycomb characteristics

Cell diameter	$d_{\text{honey}}$	10 mm
Cell length	$L_h$	70 mm
Roughness	$S_{\text{honey}}$	0.025 mm
	$L_h/D_h$	6.6
Honeycomb porosity	$\beta_h$	0.99

$$0.58 \leq \beta_s \leq 0.8 \dots\dots\dots (33)$$

The screen structure is shown in Fig. 5.

According to Fig. 5, the commonest case of square mesh is given by equation 34.

$$n_w L_{sc} d_w + n_w L_{sc} d_w - n_w (n_w d_w^2) \dots\dots\dots (34)$$

where:

$n_w$  is the number of wire,  $L_{sc}$  is the screen length,  $d_w$  is the wire diameter.

The screen porosity can be evaluated by means of equation 35.

$$\beta_s = \frac{A_{flow}}{A_{tot}} = 1 - 2 n_w \frac{d_w}{L_{sc}} + \frac{n_w^2 d_w^2}{L_{sc}^2} \dots\dots\dots (35)$$

From equation 35-36 comes out equation 36.

$$\beta_s = \left(1 - \frac{n_w d_w}{L_{sc}}\right)^2 \dots\dots\dots (36)$$

The settling chamber characteristics are shown in Table 6.

The total pressure drop inside a wind tunnel might cause due to frictional and local losses. Local losses are

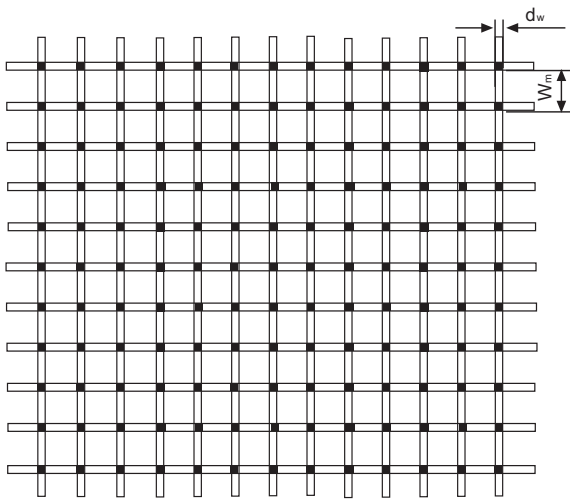


**Fig. 5.** Screen structure.

**Table 6.** Settling chamber characteristics

Wire mesh division	$W_m$	1.1 (mm)
Wire diameter	$d_w$	0.3 (mm)
	$\beta_s$	0.61

proportional to dynamic pressure and are also called dynamic losses. It can be calculated using the equation:

Dynamic loss = (Local loss coefficient) dynamic pressure

**Losses at inlet.** Losses at inlet can be found for using the given relation below for  $\alpha \leq 45^\circ$ .

$$K_{GC} = \begin{cases} 0.5 \left(1 - \frac{A_s}{A_L}\right)^{0.75} & 1.6 \sin \frac{\alpha}{2} \text{ for } 0 \leq \alpha \leq 45^\circ \\ 0.5 \left(1 - \frac{A_s}{A_L}\right)^{0.75} \sqrt{\sin \frac{\alpha}{2}} & \text{for } 45^\circ < \alpha < 180^\circ \end{cases}$$

where:

$K_{GC}$  = Pressure loss coefficient for the gradual contraction, which takes place if fluid flows from outlet to inlet:

$A_s$  = Small area

$A_L$  = Large area

$\alpha$  = Enclosed angle

The losses at the inlet are given in Table 7.

Several expressions have been derived over the years to determine the pressure drop coefficient of the screens. By using wieghardt relation for predicting K (Zheng *et al.*, 2012).

$$K = \left[6.5 \frac{1-\beta}{\beta^2}\right] \left[\frac{U_d}{\beta_v}\right]^{0.33} \dots\dots\dots (1)$$

Honeycomb loss depends on L/D ratio of honeycomb cell and porosity, while the pressure drop through the screen is dependent on the type of wire and the porosity. The losses at the screen are given in Table 8.

Then Pressure drop due to local losses:

**Table 7.** Losses at inlet

$\alpha$	$37^\circ$
$K_{GC}$	0.232

**Table 8.** Losses at screens

K-factor for screen	$K_{sc}$	0.1517
K-factor for straighteners	$K_{st}$	0.182
K-factor for diffuser	$K_{diff}$	0.763
K-factor for outlet	$K_{out}$	0.106
K-factor for nozzle	$K_{noz}$	0.232
$K_{total}$		1.435

**Table 9.** Skin friction pressure losses (Yen *et al.*, 2012)

Ducts	Air flow (m <sup>3</sup> /s)	Equivalent duct diameter (m)	Duct length (m)	Friction loss
Settling chamber	1.1	0.6	0.1	0.0284
Contraction	1.1	0.6	0.6	0.17
Test section	1.1	0.2	0.4	28.3
Diffuser	1.1	0.35	1.4	5.96
Total frictional losses	34.46 Pa			
Frictional + Local losses	1111.1 Pa			
Adding 25% (safety margin)	1.388 KPa			

$$\Delta P = 0.5 \rho K (V_{ts})^2 \dots\dots\dots (38)$$

$$\Delta P = 1076.623 \text{ Pa}$$

There are several methods to calculate the frictional losses for the ductwork. The skin friction losses are tabulated in Table 9 as determined by velocity method (Robert, 1999).

The total output power is the power required to run the wind tunnel (Wu and Ahmed, 2012).

The fan characteristics are shown in Table 10.

$$\text{Power (KW)} = \frac{K \times \text{Dynamic pressure inside a test section} \times \text{Volumetric flow rate}}{\text{Efficiency}} \dots (3)$$

The test section chamber will be made up of the transparent acrylic sheet so that the flow can be monitored with a naked eye. An opening will be introduced from which the specimen can be mounted within the chamber or can be removed, the opening will be fitted with an acrylic lid to seal the chamber as shown in Fig. 6.

Manufacturing of a contraction cone can be carried out in number of ways with various advantages and disadvantages. Potential materials are metals sheets, fibre glass and wood. Fibre glass can easily have molded into the desired shape and is very light in terms of weight. As smooth and desired finish can be obtained using fibre glass however, it will reduce the overall air friction losses ultimately. Fibre glass can be molded through many techniques, whereas the vacuum bagging

**Table 10.** Fan calculations

K (Pressure loss coefficient)	1388.85 Pa
Flowrate (m <sup>3</sup> /s)	1.1
Efficiency	0.8
Power	1.9 KW or 2.55 HP



**Fig. 6.** Acrylic test section.

technique is very popular among the vendors. To make the irregular incoming turbulent fluid flow regular, a set of sieves are put in place, otherwise known as honeycomb straighteners, due to their resemblance to a honeybee comb (Sunny *et al.*, 2020). Aluminum honeycomb straightener can be a cheap alternative for straightener, by looking at the availability of the product further techniques could also be considered like using straws or by gear pressing of metal sheets into corrugated sheets which further form a stack in a desired size as shown in Fig. 7.

Following is the final form of the complete assembly of subsonic wind tunnel as shown in Fig. 8.



**Fig. 7.** Honeycomb structure.

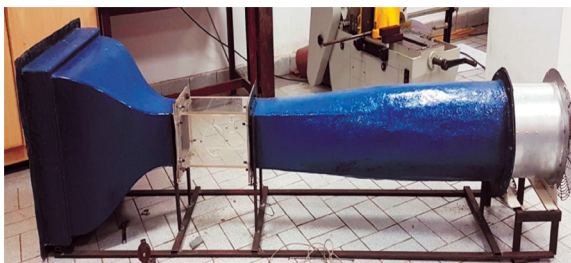


**Fig. 8.** Pictorial view of open loop subsonic wind tunnel.

## Results and Discussions

Computational Fluid Dynamics is being used to solve the defined boundary conditions calculations and simulate the fluid interaction with the surface. High speed computers with better processing capabilities can solve complex problems in shorter time. CFD is a multidisciplinary research area which interfaces the field of physics, mathematics and computer sciences. It enables the researchers to visualize the actual flow simulation. Numerical simulations allow to improve the designers of automobile and aircraft to improve the aerodynamic characteristics, military organizations to develop weapons and estimate the impact or damage (Ismail *et al.*, 2020).

CFD predicts the flow patterns which is difficult or complex to study, using traditional experiments and somehow it replicates the actual process. In actual experiment real model has to replicate inside a laboratory scale model which has numerous limits, error sources are measuring instruments and hence they are expensive to model yet they are slow and sequential. Whereas CFD simulations are cheaper, faster and parallel. They can replicate the whole model and have wide variety of operating conditions. Their error sources are usually iteration, discretization, implementation and modeling (Wu and Ahmed, 2012). But the geometry of the wind tunnel has been modeled on Creo parametric, then converted into IGS wireframe file as shown in Fig. 9.

The meshed part has been imported as ANSYS fluent 18 and boundary conditions have been applied on the named sections. The boundary conditions are shown in Table 11.

The results obtained from the overall CFD process are given below in Fig. 10.

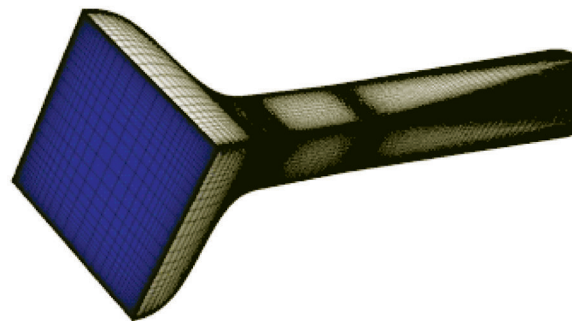


**Fig. 9.** Meshed model.

**Table 11.** Boundary conditions of the model

Model	SST k omega	
Material	Air at 25C	
	Density	1.225 Kg/m <sup>3</sup>
	Viscosity	1.5804e-5 Kg/ms
Boundary conditions	At inlet	
	Flow regime	Subsonic
	Mass flow rate	0.335 Kg/s
	Initial gauge pressure	101325 Pa
	Direction	Normal to boundary
	Turbulent intensity	3%
	Hydraulic diameter	0.6 m
	At outlet	
	Outlet gauge pressure	101325 Pa
	Solution	Backflow turbulent viscosity
Backflow turbulent viscosity ratio		2
Methods		
Scheme		Coupled
Gradient		Least square cell based
Pressure		Second order
Momentum		Second order upwind
Turbulent Kinetic energy		Second order upwind
Run calculation	Specific dissipation rates	Second order upwind
	Iterations	1000

The results we get from the experiments are given below. There are variety of tests which can be conducted in this equipment. Like the measurement of the forces applied on the airfoil inside the test section, the profile generated over the airfoil due to pressure distribution

at different speeds and angle of attack can be analyze using pressure manometers by inserting the pressure taps in the airfoil, the comparison of drag test of the golf ball and table tennis ball.

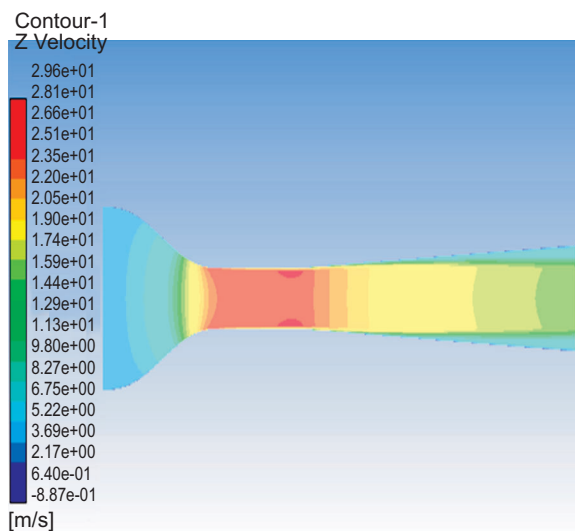


**Fig. 10.** Velocity contours of the model.

The first experiment is about the lift and drag force measurement on the airfoil at different specified speeds from (10m/s to 35m/s). Strain gauges are mounted in specific direction on the rod making a load cell, the strain gauges are connected by making a Wheatstone bridge, \ resistors connected in Wheatstone bridge should have the equal resistance as of the strain gauge (Shun and Ahmed, 2012). The Wheatstone bridge could be the quarter bridge or half or full bridge depending on the sensitivity and complexity of the instrument as shown in Fig. 11.

The load cell is attach to the servo motor and it is mounted outside the test section, after calibration of the whole equipment the sweep command is used to vary angle of attack of the airfoil, though we can plot the variation of forces. We used NACA 0012 as our first test the specimen. The results of tests are shown in Table 12 and Fig. 12-13.

**Table 12.** Lift and drag test

AOA (C°)	Lift force (N)	Drag force (N)	Coefficient of lift	Coefficient of drag
-10	-1.72	0.055	-0.53855	0.02992
-5	-0.99	0.03	-0.9411	0.01632
0	0.037	0.012	0.020128	0.006528
5	1.14	0.028	0.62015	0.015232
10	1.76	0.05	0.957424	0.0272

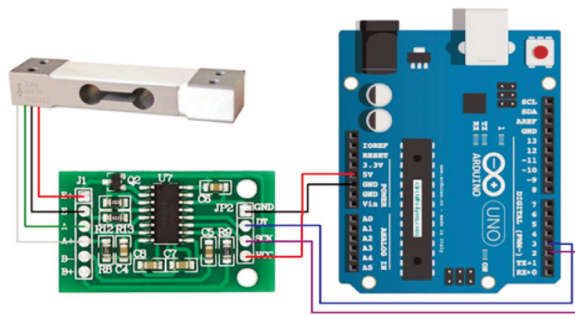


**Fig. 11.** Load cell connections to HX711 and Arduino.

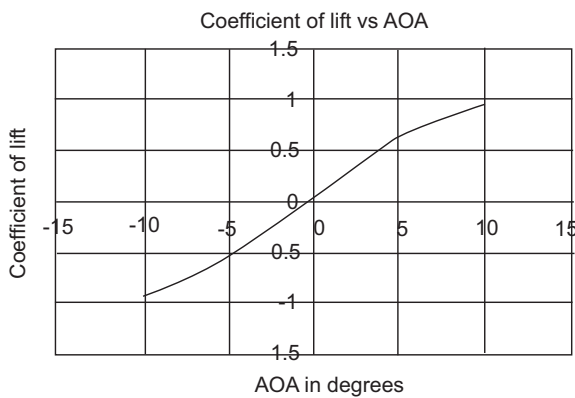


**Fig. 12.** Coefficient of lift vs angle of attack.

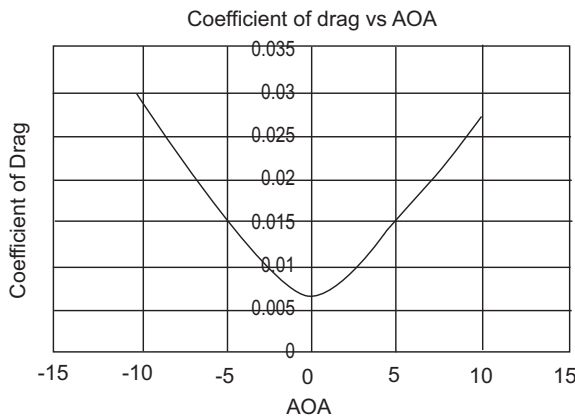


**Fig. 13.** Coefficient of drag vs angle of attack.

**Conclusion**

This research aimed to design and fabricate a low-speed open loop subsonic wind tunnel for educational purpose. In the wind tunnel air is sucked through the fan at the exit and air enters through settling chamber where air gets uniform and completes the loop. Test section speed was selected to be Mach 0.1 since it is enough to assist the aerodynamic test requirements of student-based projects. Whereas speed inside the test section can be attenuated as per the availability of fan in our region, fiberglass is being considered as the best material due to its availability and ease of molding. The aim is to keep instrumentation as smart as possible in limited budget. More electronic instruments are preferred to make it user-friendly and keep it as affordable.

**Conflict of Interest.** The authors declare no conflict of interest.

**References**

Abdelhamed, S., Yassen, Y., ElSakka, M. 2015. Design optimization of three dimensional geometry of wind tunnel contraction. *Ain Shams Engineering Journal*, **6**: 281-288. <https://www.sciencedirect.com/science/article/pii/S2090447914001221>

Ahmed, N.A. 2010. Wind driven natural-solar/electric hybrid ventilators, *Wind Power, Section D: The Environmental Issues*, In-Tech Organization, Austria. <https://www.intechopen.com/books/wind-power/wind-solar-driven-natural-electric-hybrid-ventilators>

Ahmed, N.A. 2012. Novel developments towards efficient and cost effective wind energy generation and utilization for sustainable environment. *Renewable and Power Quality Journal*, **10**: 11-31. <https://www.semanticscholar.org/paper/Novel-developments-towards-efficient-and-cost-wind-Ahmed/17a2118c10ae75642fa36b032c7543ad34666a74>

Almeida, O., Miranda, F.C., Ferreira, Neto, O., Saad, F.G. 2018. Low subsonic wind tunnel – design and

- construction. *Journal of Aerospace Technology and Management*, **10**: 1-10. [https://www.researchgate.net/publication/323408885\\_Low\\_Subsonic\\_Wind\\_Tunnel\\_-\\_Design\\_and\\_Construction](https://www.researchgate.net/publication/323408885_Low_Subsonic_Wind_Tunnel_-_Design_and_Construction)
- Blevins, R. 1986. *Nozzles, Diffusers and Venturis. Applied Fluid Dynamics Handbook*, pp. 144-163. <https://www.worldcat.org/title/applied-fluid-dynamics-handbook/oclc/560643298>
- Eugeni, M., Elahi, H., Fune, F., Lampani, L., Mastroddi, F., Romano, G.P., Gaudenzi, P. 2020. Numerical and experimental investigation of piezoelectric energy harvester based on flag-flutter. *Aerospace Science and Technology*, **97**: 105634. [https://iris.uniroma1.it/retrieve/handle/11573/1361147/1357180/Eugeni\\_Preprint\\_Numerical%20and%20experimental\\_2020.pdf.pdf](https://iris.uniroma1.it/retrieve/handle/11573/1361147/1357180/Eugeni_Preprint_Numerical%20and%20experimental_2020.pdf.pdf)
- Findanis, N., Ahmed, N. A. 2011. Wind tunnel 'concept of proof' investigations in the development of novel fluid mechanical methodologies and devices', invited Chapter in *Wind Tunnels and Experimental Fluid Dynamics Research*, In-Tech Organization, Austria. <https://www.intechopen.com/books/wind-tunnels-and-experimental-fluid-dynamics-research/wind-tunnel-concept-of-proof-investigations-in-the-development-of-novel-fluid-mechanical-methodologi>
- Hernandez, G., Lopez, M., Perales, P., Wu, Y., Xiaoxiao, S. 2013. Design methodology for a quick and low-cost wind tunnel, *Wind Tunnel Designs and Their Diverse Engineering Applications*, Book Chapter, pp. 3-28. <https://www.semanticscholar.org/paper/Chapter-1-Design-Methodology-for-a-Quick-and-Wind-Hern%C3%A1ndezL%C3%B3pez/be24f6fe617d03fd1c88c3c9c17aec71ed6b4d2e>
- Hernández, G., López, A., Jarzabek, J., Perales, M., Wu, Y. 2011. Design methodology for a quick and low-cost wind tunnel, *Wind Tunnel Designs and Their Diverse Engineering Applications*, pp. 3-28. <https://www.intechopen.com/books/wind-tunnel-designs-and-their-diverse-engineering-applications/design-methodology-for-a-quick-and-low-cost-wind-tunnel>
- Ismail, J.J., Pane, E., Suyitno, B.M., Rahayu, G., Rhakasywi, D., Suwandi, A. 2020. Computational fluid dynamics simulation of the turbulence models in the tested section on wind tunnel. *Ain Shams Engineering Journal*, **11**: 12011209. <https://www.sciencedirect.com/science/article/pii/S2090447920300484>
- Joglekar, B., Mourya, R. 2014. Design, construction and testing open circuit low speed wind. *International Journal of Electrical and Electronics Research*, **2**: 1-9. <https://www.semanticscholar.org/paper/DESIGN%2C-CONSTRUCTION-AND-TESTING-OPEN-CIRCUIT-LOW-Joglekar-Mourya/f402d604e3e626412e33f046aaf43d423d44c356>
- Kumar, S., Dwivedi, V., Kumar, J., Goswami, R. 2012. Design and simulation of open circuit blowdown type wind tunnel. In: *Proceedings of the fourth International Congress on Computational Mechanics and Simulation (ICCMS 2012)*, IIT Hyderabad, India, pp. 10-12. [https://www.researchgate.net/publication/236154652\\_Design\\_and\\_simulation\\_of\\_Open\\_Circuit\\_Blowdown\\_type\\_Wind\\_Tunnel](https://www.researchgate.net/publication/236154652_Design_and_simulation_of_Open_Circuit_Blowdown_type_Wind_Tunnel)
- Leifsson, L., Koziel, S. 2015. Simulation-driven design of low-speed wind tunnel contraction. *Journal of Computer Science*, **7**: 1-12. [https://www.researchgate.net/publication/270596007\\_Simulation-Driven\\_Design\\_of\\_Low-Speed\\_Wind\\_Tunnel\\_Contraction](https://www.researchgate.net/publication/270596007_Simulation-Driven_Design_of_Low-Speed_Wind_Tunnel_Contraction)
- Lerner, J., Boldes, U. 2011. *Wind Tunnels and Experimental Fluid Dynamics Research*, Book Chapter, pp. 1661-2345. <https://www.intechopen.com/books/wind-tunnels-and-experimental-fluid-dynamics-research>
- Lien, J., Ahmed, N.A. 2011. *Wind Driven Ventilation for Enhanced Indoor Air Quality*, Invited Chapter, in 'Chemistry, Emission, Control, Radioactive Pollution and Indoor Air Quality', edited by Nicholas A Mazzeo, In-Tech Organization, Austria. <https://www.intechopen.com/books/chemistry-emission-control-radioactive-pollution-and-indoor-air-quality/wind-driven-ventilation-for-enhanced-indoor-air-quality>
- Madara, S.R., Varghese, J.T., Selvan, M.C.P. 2017. Design and fabrication of low cost open circuit subsonic wind tunnel. *International Journal of Innovative Technology and Research*, **5**: 6154-6161. [https://www.researchgate.net/publication/318959900\\_Design\\_and\\_Fabrication\\_of\\_Low\\_Cost\\_Open\\_Circuit\\_Subsonic\\_Wind\\_Tunnel](https://www.researchgate.net/publication/318959900_Design_and_Fabrication_of_Low_Cost_Open_Circuit_Subsonic_Wind_Tunnel)
- Maurya, N.K., Maurya, M., Tyagi, A., Dwivedi, S.P., 2018. Design and fabrication of low speed wind tunnel and flow analysis. *International Journal of Engineering & Technology*, **7**: 381-387. [https://www.researchgate.net/publication/329872818\\_Design\\_Fabrication\\_of\\_Low\\_Speed\\_Wind\\_Tunnel\\_and\\_Flow\\_Analysis](https://www.researchgate.net/publication/329872818_Design_Fabrication_of_Low_Speed_Wind_Tunnel_and_Flow_Analysis)
- Mashud, M. 2012. Design construction and performance

- test of a low cost subsonic wind tunnel. *IOSR Journal of Engineering*, **10**: 83-92. [https://www.researchgate.net/publication/271251293\\_Design\\_Construction\\_and\\_Performance\\_Test\\_of\\_a\\_Low\\_Cost\\_Subsonic\\_Wind\\_Tunnel](https://www.researchgate.net/publication/271251293_Design_Construction_and_Performance_Test_of_a_Low_Cost_Subsonic_Wind_Tunnel)
- Nguyen, Q. 2014. Designing, constructing and testing a low – speed open –jet wind tunnel. *International Journal of Engineering Research and Applications*, **4**: 243-246. [http://www.ijera.com/papers/Vol4\\_issue1/Version%202/AG4102243246.pdf](http://www.ijera.com/papers/Vol4_issue1/Version%202/AG4102243246.pdf)
- Paper, C., Chauhan, J., University, P. 2012. Design and simulation of open circuit blowdown type wind tunnel. In: *Proceedings of the Fourth International Congress on Computational Mechanics and Simulation (ICCMS 2012)*, IIT Hyderabad, India. [https://www.researchgate.net/publication/236154652\\_Design\\_and\\_simulation\\_of\\_Open\\_Circuit\\_Blowdown\\_type\\_Wind\\_Tunnel](https://www.researchgate.net/publication/236154652_Design_and_simulation_of_Open_Circuit_Blowdown_type_Wind_Tunnel)
- Parpanchi, S.M., Farsad, S., Ardekani, M.A., Farhani, F. 2021. Experimental investigation of a diffuser for use in skydiving vertical wind tunnel. *Experimental Thermal and Fluid Science*, **125**: 110393. <https://www.sciencedirect.com/science/article/abs/pii/S0894177721000443>
- Riazi, H., Ahmed, N. 2011. Numerical investigation on two-orifice synthetic jet actuators of varying orifice spacing and diameters. In: *Proceeding of the 29<sup>th</sup> AIAA Applied Aerodynamics Conference*, Honolulu, Hawaii, USA. <https://arc.aiaa.org/doi/10.2514/6.2011-3171>
- Robert, A. Parsons (ASHRAE Handbook Editor), 1999. *ASHRAE Fundamental Handbook*, p. 851. <https://www.pdfdrive.com/ashrae-handbook-1997-fundamentals-e158435229.html>
- Shun, S., Ahmed, N.A. 2012. Wind turbine performance improvements using active flow control techniques. In: *Procedia Engineering, Elsevier Publications*, **49**: 83-91. <https://www.sciencedirect.com/science/article/pii/S1877705812047728>
- Singh, M., Singh, N., Yadav, S. 2013. Review of design and construction of an open circuit low speed wind tunnel. *Global Journal of Researches in Engineering: Mechanical and Mechanics Engineering*, **13**: 1-21. <https://www.semanticscholar.org/paper/Review-of-Design-and-Construction-of-an-Open-Low-Singh-Singh/6ba2b7c43e574bac6f3ecd67c42e53bd72fcc77b>
- Sunny, K.A., Kumar, P., Kumar, N.M. 2020. Experimental study on novel curved blade vertical axis wind turbines. *Results in Engineering*, **7**: 100149. <https://www.sciencedirect.com/science/article/pii/S2590123020300554>
- Verma, N., Baloni, B.D. 2018. Numerical and experimental investigation of flow in an open-type subsonic wind tunnel. *SN Applied Sciences*, **1**: 1-12. <https://link.springer.com/article/10.1007%2Fs42452-019-1422-3>
- Wu, C., Ahmed, N. 2012. Novel mode of air supply for aircraft cabin ventilation. *Building and Environment*, **56**: 45-56. <https://www.sciencedirect.com/science/article/abs/pii/S0360132312000704>
- Yen, J., Ahmed, N. 2012. Parametric study of dynamic stall flow field with synthetic jet actuation. *Journal of Fluids Engineering, Transactions of the ASME*, **134**: 45-53. <https://asmedigitalcollection.asme.org/fluidsengineering/article-abstract/134/7/071106/456352/Parametric-Study-of-Dynamic-Stall-Flow-Field-With?redirectedFrom=fulltext>
- Yen, J., Ahmed, N. 2013. Synthetic jets as a boundary vorticity flux control tool. *AIAA Journal*, **51**: 510-513. <https://arc.aiaa.org/doi/abs/10.2514/1.J051797?journalCode=aiaaj>
- Zheng, Y., Ahmed, A., Zhang, W. 2012. Impact analysis of varying strength counter-flow jet ejection on a blunt shaped body in a supersonic flow. *Advances and Applications in Fluid Mechanics*, **12**: 119-129. [https://www.researchgate.net/publication/267082749\\_Impact\\_analysis\\_of\\_varying\\_strength\\_counter-flow\\_jet\\_ejection\\_on\\_a\\_blunt\\_shaped\\_body\\_in\\_a\\_supersonic\\_flow](https://www.researchgate.net/publication/267082749_Impact_analysis_of_varying_strength_counter-flow_jet_ejection_on_a_blunt_shaped_body_in_a_supersonic_flow)